Turkish Journal of Electrical Engineering & Computer Sciences

http://journals.tubitak.gov.tr/elektrik/

Research Article

Turk J Elec Eng & Comp Sci
(2016) 24: 2336 – 2348

doi:10.3906/elk-1402-239

# Theoretical analysis of doping management and its effects on power scaling

**Amira TANDİROVİÇ GÜRSEL[1,*], Parviz ELAHİ[2], Fatih Ömer İLDAY[3], Mustafa Sadettin ÖZYAZICI[4]**

[1]Department of Electrical and Electronics Engineering, Adana Science and Technology University, Adana, Turkey
[2]ARL Building, Bilkent University, Ankara, Turkey
[3]SL-101 (ARL Building), or EE-506 (EE Building), Bilkent University, Ankara, Turkey
[4]Department of Electrical and Electronics Engineering, Bahçeşehir University, İstanbul, Turkey

**Received:** 21.02.2014 • **Accepted/Published Online:** 10.07.2014 • **Final Version:** 15.04.2016

**Abstract:** Thermal load and nonlinear effects are two contrary phenomena that make up important drawbacks in rapid progress of high-power fiber lasers. To minimize the thermal load, which limits the average power, doping concentration should be decreased, which brings about increasing length of the fiber. In contrast, the presence of nonlinear effects and their management demand the use of high-doped, shorter fibers in order to maximize the peak power. Management on doping of gain fiber and obtaining a specific doping profile function along the short gain fiber is a proposed solution for prevention of the exchange between thermal load and nonlinear effects. The study shows two different approaches for keeping the temperature levels down in addition to obtaining power scaling profiles.

**Key words:** Double-clad fiber lasers, doping profile function, thermal management, power scaling

## 1. Introduction

Although fiber lasers have drawn considerable attention since their rediscovery by Payne and co-workers in 1985 [1], the progress, aided by fruitful and abundant experimental and theoretical results, has come of age over the last decade [2,3]. This astonishingly rapid progress has resulted in a wide range of configurations, spectral ranges, and temporal formats, and they are now leading candidates for many important applications requiring powers progressed from a few watts up to multi-kilowatts [3–5] and even more than a megawatt today [6]. The motivation for the intensive research and development in fiber laser technology has been driven by the permanently growing market whose trailblazer is the telecommunication industry [7]. Although high-power fiber lasers (HPFLs) were originally developed for telecom applications, researchers have also driven numerous different applications in medicine [8], remote sensing [5], material processing [9], etc., due to a number of intrinsic advantages, including simplicity of optical cavity construction, high efficiency, excellent beam quality, and microjoule-level energies at high repetition rates that boost processing speed [10].

With few exceptions, HPFLs are rare-earth-doped silica fibers with the double clad concept, carried out in 1988, pumped by multimode diode sources that still produce single-mode output [10,11]. Among various rare-earth-doped materials, erbium (Er), ytterbium (Yb), neodymium (Nd), and thulium (Tm) are frequently chosen primarily because of their appropriate characteristics in terms of spectroscopy, solubility, efficiency etc. [11,12]. However, $Yb^{+3}$ has come to the fore because of some important advantages such as the long life-time

*Correspondence: agursel@adanabtu.edu.tr

of the excited state and the simple energy level scheme, and the extensionally low quantum defect between the pump and laser wavelength [13] leads to high efficiency that may exceed 80%, which is of extreme importance for reduction of heat generation [14].

For small power levels, below 1 kW, thermal problems have been of little concern as the pumping radiation converted into heat is small enough that they can be neglected or overtaken by several simple strategies for mitigating the thermal lensing and the stress induced birefringence effects or simply cooling at the pump power launching end [15,16]. However, strong demand for increase in output power has led to impressive progress in fiber diversity, which has driven up the thermal rise that can no longer be ignored. It has been addressed particularly since high power 1.5 *mu* m signal was generated [16,17]. Owing to this, many resources have been focused on the cooling process followed by the discovery of many different kinds of cooling techniques and approaches [18,19]. In this sense, it can be deduced that a prominent way of cooling is the introduction of a particular cooling process of gain fibers at different wavelengths.

At first, it gave the misleading impression that choosing the appropriate cooling process is enough to get rid of thermal limitations due to thermal load spreads over meter or 10 meter long fibers that is enough to avoid those limitations.

However, as power scaling has progressed over time, fiber lasers have become shorter in order to maximize the peak power. Actually, from a historical point of view, breaking the 1 kW barrier in 2002 has been one of the most important milestones in the evolution of fiber lasers [4]. Since then, astonishingly rapid progress in pumping configurations [20–22], cooling techniques and technologies [23,24], fiber design, an fabrication as well as the fundamental fiber geometry itself [25], has led to an unprecedented increase in the average power. Hence, heating and its beam-distorting effects have become again a current issue as the powers continue to increase for very short high-power lasers due to heavy thermal load that can give rise to permanent defects on the clad and coating materials [26,27]. In order to overcome thermal defects, several geometries of the gain media, such as disc and slab as well as some other thermal reduction objected geometries, have been developed [28,29]. Likewise, a significantly improvement has been achieved by breaking of the cylindrical symmetry of the inner cladding, carefully studied by many researchers among which are Limpert, Tünnermann, and co-workers [4,29].

In spite of the efforts of many resources to overcome the thermal limitations by the fiber architecture, the resource progress soon scrolled toward thermal analysis and calculations of internal thermal distribution based on heat flux approximations [30]. Early studies considered only convective heat transfer neglecting longitudinal variation over the fiber length. That reasonable and close to reality approximation, based on averaging the thermal load over the length, was appropriate for 2-D simulations of long fibers with small pump absorption coefficient [30–32]. However, soon, with the presence of nonlinear effects, it was noted that such treatment for the much shorter length of the active fibers may bring about a rather large calculation error. The main reason is that in short-length fiber lasers the axial temperature changes significantly as a result of the exponential changing of thermal load in the longitudinal direction [33], resulting in the emergence of an important drawback of the 2-D frame approach concerned with the plain-strain approximation of calculating thermal stress [33,34]. As 2-D flux approximation came up short in modeling of thermal load of the short length fiber lasers, the need for a comprehensive 3-D analysis of thermal effects was underlined [35–37].

There is no doubt that all of the foregoing methods are very important but it is also quite certain that they will fall short to catch up with continually increasing average power levels. Therefore, it may be deduced that it is needed to find some additive method to take heat under control. Herein, a doping management approach [38], revealed by Ilday and colleagues, can be a promising method for further research.

This study is a theoretical analysis of doping management in terms of thermal load, according to the thermal conductive equations taking into account natural and geometrical properties of the fiber medium as well as the pump beam intensity profile. Thermal equations derived for the core and the clad as well as the pump beam intensity profile have been considered from two different points: constant and variable absorption coefficients.

## 2. Rate equations

Most linear-cavity Yb-doped double-clad fiber lasers use one of two pumping configurations types: single or double-end configuration explained in [39]. A typical high power single-end pumped fiber laser, with reflectors at both sides, is illustrated in Figure 1.

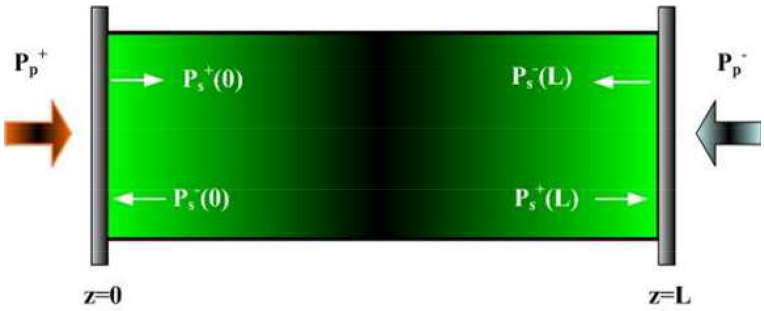


**Figure 1.** Schematic illustration of a typical end-pumped $Yb^{3+}$-doped double-clad fiber laser.

The forward and backward propagation beams satisfy the steady-state rate equations that are given through three equations [39,40]:

$$\frac{\partial N_2(z,t)}{\partial t} = \left(\frac{\lambda_p \Gamma_p \delta_{pa}}{hcA}\right)[N - N_2(z.t)]\left[P_p^+(z,t) + P_p^-(z,t)\right] -$$

$$-\left(\frac{\lambda_p \Gamma_p \delta_{pe}}{hcA}\right) N_2(z.t)\left[P_p^+(z,t) + P_p^-(z,t)\right] - \left(\frac{\lambda_p \Gamma_p \delta_{pe}}{hcA}\right) N_2(z.t)\left[P_s^+(z,t) + P_s^-(z,t)\right] +$$

$$+\left(\frac{\lambda_p \Gamma_p \delta_{pa}}{hcA}\right)[N - N_2(z.t)]\left[P_s^+(z,t) + P_s^-(z,t)\right] -$$

$$-\frac{N_2(z,t)}{\tau} \tag{1}$$

$$\pm\frac{dP_s^{\pm}}{dz}(z,t) = \Gamma_s\left[(\sigma_{se} + \sigma_{sa})N_2(z,t) - \sigma_{sa}N\right]P_s^{\pm}(z,t) - \alpha_s P_s^{\pm}(z,t) \tag{2}$$

$$\pm\frac{dP_p^{\pm}}{dz}(z,t) = \Gamma_p\left[(\sigma_{se} + \sigma_{sa})N_2(z,t) - \sigma_{sa}N\right]P_p^{\pm}(z,t) - \alpha_s P_p^{\pm}(z,t) \tag{3}$$

where $N_2(z,t)$ is the upper laser level population density with spontaneous lifetime $\tau$, $A$ is a cross-section area of the core, $N$ is the dopant concentration in the core, $h$ is Planck's constant, and $c$ is the speed of light in a vacuum. $P_p^{\pm}$, $_p$, $\Lambda_p$, $P_s^{\pm}$, $\Lambda_s$, and $\lambda_s$ denote powers, filling factors, and laser wavelengths for the pump and signal, respectively. The positive and negative superscripts represent forward and backward pumping configurations, respectively [41].

Referring to (2) and (3), $\sigma_{pa}$,$\sigma_{pe}$, $\sigma_{sa}$, and $\sigma_{se}$ are the absorption and emission cross sections at the pump and signal wavelengths, respectively, while $\alpha_s$ and $\alpha_p$ represent attenuation coefficients of the signal and pump light [41,42].

For a fiber laser, the rate equations have to be solved according to the boundary conditions of the laser cavity given as [43,44]:

$$P_s^+(0) = R_1 P_s^-(0) \tag{4}$$

$$P_s^-(L) = R_1 P_s^+(L), \tag{5}$$

where $L$ is the length of the fiber and $R_1$ and $R_2$ are the power reflectivity at the lasing wavelength $\lambda$ of the forward and backward cavity mirrors, respectively. The reflectivity of the mirrors is assumed to be minimal for $\lambda = \lambda_p$ and maximal for $\lambda = \lambda_s$ [43]. As the heat source in a fiber laser mainly depends on the absorption and loss of pump light, Eq. (3) may be reformulated as [33]

$$\pm \frac{dP_p^{\pm}}{dz}(z,t) = -[\alpha_a(z) + \alpha_s] P_p^{\pm}(z,t), \tag{6}$$

where $\alpha_\alpha(z)$ is absorption coefficient expressed as

$$\alpha_a(z) = -\Gamma_p [(\sigma_{se} + \sigma_{sa}) N_2(z,t) - \sigma_{sa} N] \tag{7}$$

Although it is generally accepted that backward pumping can yield higher gain at high powers, the research is focused on forward pumping since that has two important advantages over backward pumping: lower thermal load and better power stabilization [43]. Maximal signal and pump powers are reached at opposite ends of the fiber, resulting in the lower thermal load. In spite of reduction of the B integral over the gain fiber, this is more than stabilization by propagation in undoped fibers that is necessary for all-fiber pump delivery [38]. It is to be mentioned that propagation in passive fiber is more harmful than in gain fiber, as spectral broadening is restricted by gain filtering.

Particularly, the time independent forward-end pumped top-hat profile, which is, in the thermal point of view, superior to other profiles used in high power forward end-pumped systems, is given by [45]

$$P(z) = \xi P_o exp(-a(z)z) \tag{8}$$

Thus for forward-end pumped top-hat shape profile,

$$\frac{dP_p^+}{dz}(z) = -a(z)\xi P_o exp(-a(z)z), \tag{9}$$

where $a(z) = \alpha_a(z) + \alpha_s$.

## 3. Theoretical analysis of the heat dissipation mechanism

Fiber temperature, originated from conversion of a fraction of pump energy during operation, is a 3-D boundary value problem with the core acting as a heat source. The inner and outer claddings can be considered as one body since no source is represented in the cladding region, resulting in secondary effects of outer cladding that can be ignored. The 3-D thermal distribution model for double-clad fiber is shown in Figure 2. $r$ is the radial coordinate, $\varphi$ is the tangential angle, and $z$ is the axial coordinate. The quantities $\boldsymbol{a}$ and $\boldsymbol{b}$ are core cladding radii, respectively [30].

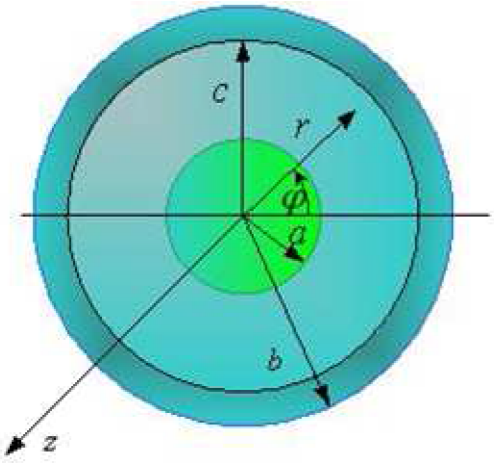


**Figure 2.** Geometry of modeled double-clad fiber.

The steady-state heat equations for both core and cladding regions are given as follows [24,36,37]:

$$\frac{1}{r}\frac{\partial}{\partial r}\left(r\frac{\partial T_1(r,z)}{\partial r}\right)+\frac{\partial^2 T_1(r,z)}{\partial z^2}=-\frac{Q(r,z)}{k_f};0\le r\le a \tag{10}$$

$$\frac{1}{r}\frac{\partial}{\partial r}\left(r\frac{\partial T_2(r,z)}{\partial r}\right)+\frac{\partial^2 T_2(r,z)}{\partial z^2}=0;a\le r\le b \tag{11}$$

It is to be noted that the azimuthal variation of the temperature is ignored due to the cylindrical symmetry of the fiber [24]. $T1(r,z)$ and $T2(r,z)$ are the temperatures in the core and cladding regions, respectively. In Eq. (10) $kf$ denotes the thermal conductivity of the fiber, while $Q(r,z)$ is the heat density given as a function of radius and propagation distance. For the forward-end top-hat profile the heat source density function can be represented as [43]

$$Q(rz)=\frac{\xi}{\pi a^2}P_o a(z)exp(-a(z)z), \tag{12}$$

where $P_o$ denotes the pump power, $a(z)$ is the pump absorption coefficient, and $\xi$ is the fractional thermal load or the conversion coefficient that appears due to the quantum defect [42].

In (11) the right side of the equation is zero as no source is represented. Temperature functions from (10) and (11) have to be solved using the method of separating variables with transformation $T(r,z)=\varphi(r)\theta(z)$, taking into account that temperature function has two separable components in radial and axial directions [36,37]. The differential equations to be solved are two separately differential equations with and without source, respectively.

$$\frac{1}{r\varphi_1(r)}\frac{\partial}{\partial r}\left(r\frac{\partial\varphi_1(r)}{\partial r}\right)+\frac{1}{\theta_1(z)}\frac{d^2\theta_1(z)}{dz^2}=-\frac{\xi P_0\alpha(z)}{k_f\pi a^2}\frac{exp?(-\alpha(z)z)}{\varphi_1(r)\theta_1(z)} \tag{13}$$

$$\frac{1}{r\partial\varphi_2}\frac{\partial}{\partial r}\left(r\frac{\partial\varphi_2(r)}{\partial r}\right)+\frac{1}{\theta_2(z)}\frac{d^2\theta_2(z)}{dz^2}=0 \tag{14}$$

It is to be noted that both sides of Eqs. (13) and (14) are divided by $\varphi(r)\,\theta(z)$. As the absorption coefficient is variable along of z, Eq. (13) is as such insolvable. Because of this, the fiber is considered as a system divided into each L/n length long n subsystems along the fiber axis where L is the length of the fiber. For large values of n, all of the subsystems act as separate part that absorption coefficient can be treated as constant. It is important to notify that, in terms of both power and temperature, the input of each subsystem, except the first one, is the output of the previous one. Therefore, the pumping distribution of the i-th subsystem, where $1 \leq i \leq n$, can be represented as

$$P_i = P_{(i-1)} exp(-\alpha_i \frac{L}{n}) = P_0 exp(-\frac{L}{n}\sum_{j=1}^{i}\alpha_j) \tag{15}$$

Taking to account this property, Eqs. (4) and (5) can be rewritten as

$$\frac{1}{r\varphi_{1i}(r)}\frac{\partial}{\partial r}\left(r\frac{\partial\varphi_{1i}(r)}{\partial r}\right) + \frac{1}{\theta_{1i}(z)}\frac{d^2\theta_{1i}(z)}{dz^2} = -\frac{\xi P_i\alpha_i}{k_f\pi a^2}\frac{exp?(-\alpha_i z_i)}{\varphi_{1i}(r)\theta_{1i}(z)} \tag{16}$$

$$\frac{1}{r\partial\varphi_{2i}}\frac{\partial}{\partial r}\left(r\frac{\partial\varphi_{2i}(r)}{\partial r}\right) + \frac{1}{\theta_{2i}(z)}\frac{d^2\theta_{2i}(z)}{dz^2} = 0, \tag{17}$$

where $z_i = i\frac{L}{n}$.

For axial parts represented in exponential decay form $\theta_{1i}(z) = \exp?(-\alpha_i z_i)$, $\theta_{2i}(z) = \exp?(-\beta_i z_i)$, and $\eta_i = \xi P_i\alpha_i / k_f\pi a^2$ equations are transformed into modified zero-order Bessel and zero-order Bessel equations, respectively, as given below:

$$\frac{1}{r\varphi_{1i}(r)}\frac{\partial}{\partial r}\left(r\frac{\partial\varphi_{1i}(r)}{\partial r}\right) + \alpha_i^2 = -\frac{\eta_i}{\varphi_{1i}(r)} \tag{18}$$

$$\frac{1}{r\varphi_{2i}(r)}\frac{\partial}{\partial r}\left(r\frac{\partial\varphi_{2i}(r)}{\partial r}\right) + \beta_i^2 = 0 \tag{19}$$

Therefore, solutions for the radial parts of the temperature functions with and without source are

$$\varphi_{1i} = a_{1i}J_0(\alpha_i r) - a_{2i}Y_0(\alpha_i r) - \frac{\eta_i}{\alpha_i^2} \tag{20}$$

$$\varphi_{2i} = b_{1i}J_0(\beta_i r) - b_{2i}Y_0(\beta_i r) \tag{21}$$

Hence, the temperatures of i-th subsystem can be represented as

$$T_{1i}(rz_i) = \eta_i\left[A_{1i}J_0(\alpha_i r) - A_{2i}Y_0(\alpha_i r) - \frac{1}{\alpha_i^2}\right]\exp(\alpha_i z_i) + Tc \tag{22}$$

$$T_{2i}(r, z_i) = \eta_i\left[B_{1i}J_0(\beta_i r) - B_{2i}Y_0(\beta_i r)\right]\exp(\beta_i z_i) + Tc \tag{23}$$

$A_{1i}A_{2i}, B_{1i}$, and$B_{2i}$ are arbitrary constants to be determined from boundary conditions given below [30,33,36,37].

$$\partial T_1(r, z_i)|_{r=0} = finite \tag{24}$$

$$T_1(r,z_i)|_{r=a} = T_2(r,z_i)|_{r=a} \tag{25}$$

$$\int_V Q(r,z_i)dV = \int_S k_c \left.\frac{\partial T_2(r,z_i)}{\partial r}\right|_{r=b} dS \tag{26}$$

$$\left.\frac{\partial T_2(r,z_i)}{\partial r}\right|_{r=b} = \frac{h}{k_c}\left(T_c - T_2(r,z_i)|_{r=b}\right). \tag{27}$$

$k_c$, $T_c$, and $h$ are the thermal conductivity, the cooling temperature, and the convective coefficient of the surface, respectively. From conditions (23) and (24) it is found that $A_{2i}$ has to be zero as well as $\alpha_i = \beta_i$. Hence, the relation between $A_{1i}$ , $B_{1i}$, and $B_{2i}$ can be expressed as

$$A_{1i} = B_{1i} - B_{2i}\frac{Y_0(\alpha_i a)}{J_0(\alpha_i a)} + \frac{1}{J_0(\alpha_i a)\,\alpha_i^2} \tag{28}$$

The relation between $B_{1i}$, and $B_{2i}$ can be obtained by introducing the definition for the derivative of the Bessel function in condition (17)

$$B_{1i}J_1(\alpha_i b) - B_{2i}Y_1(\alpha_i b) = \frac{a^2}{2bK\alpha_i}, \tag{29}$$

where $K = k_c/k_f$

From condition (18) it is found that

$$B_{2i} = \frac{hJ_0(\alpha_i b) - k_c\alpha_i J_1(\alpha_i b)}{hY_0(\alpha_i b) - k_c\alpha_i Y_1(\alpha_i b)}B_{1i} \tag{30}$$

Using relations for cross-products of Bessel functions [46], Eqs. (28), (29), and (30) form an equation set whose solutions are found to be:

$$A_{1i} = \frac{a^2\left(J_0(\alpha_i a) - \gamma Y_0(\alpha_i a)\right)}{2bK\alpha_i J_0(\alpha_i a)\left(J_1(\alpha_i b) - \gamma Y_1(\alpha_i b)\right)} + \frac{1}{\alpha_i^2 J_0(\alpha_i a)} \tag{31}$$

$$B_{1i} = \frac{\pi a^2}{4bh}\left(hY_0(\alpha_i b) - k_c\alpha_i Y_1(\alpha_i b)\right) \tag{32}$$

$$B_{2i} = \frac{\pi a^2}{4bh}\left(hJ_0(\alpha_i b) - k_c\alpha_i J_1(\alpha_i b)\right), \tag{33}$$

where $\gamma = \frac{hJ_0(\alpha_i b) - k_c\alpha_i J_1(\alpha_i b)}{hY_0(\alpha_i b) - k_c\alpha_i Y_1(\alpha_i b)}$

Finally, using Eqs. (22), (23), (31), and (33), 3-D analytical solutions for the temperature distribution at core and clad regions, respectively, for variable absorption coefficient, are obtained as follows [47]:

$$T_{1i}(r,z_i) = \frac{\xi\alpha_i}{k_f\pi a^2}P_0 exp\left(-\frac{L}{n}\sum_{j=1}^{i}\alpha_j\right) \times$$

$$\left[\left(\frac{a^2\left(J_0\left(\alpha_i a\right)-\gamma Y_0\left(\alpha_i a\right)\right)}{2bK\alpha_i J_0\left(\alpha_i a\right)\left(J_1\left(\alpha_i b\right)-\gamma Y_1\left(\alpha_i b\right)\right)}+\frac{1}{\alpha_i^2 J_0\left(\alpha_i a\right)}\right)J_0\left(\alpha_i r\right)-\frac{1}{\alpha_i^2}\right]\exp\left(-\alpha_i z_i\right)+Tc \tag{34}$$

$$T_{2i}\left(r,z_i\right)=\frac{\xi\alpha_i}{4bhk_f}P_0 exp\left(-\frac{L}{n}\sum_{j=1}^{i}\alpha_j\right)\times$$

$$\left[\left(hY_0\left(\alpha_i b\right)-k_c\alpha_i Y_1\left(\alpha_i b\right)\right)J_0\left(\alpha_i r\right)-\left(hJ_0\left(\alpha_i b\right)-k_c\alpha_i J_1\left(\alpha_i b\right)\right)Y_0\left(\alpha_i r\right)\right]$$

$$\exp\left(-\alpha_i z_i\right)+Tc \tag{35}$$

At z = 0 the heat in the core and cladding can be found using 2-D analysis for double-clad fibers represented in [37].

## 4. Results and discussion

The materials used for low-index polymer coatings of conventional double-clad fibers are very sensitive to high thermal loads, especially when they are exposed for a long time. Although most of them have higher damage temperatures, generally varying between 150 and 200 $^{circ}$ C, it is to be noted that long-term reliability may require operation below 80 $^{circ}$ C (253.1 K) [26]. Additionally, considerable heating may change properties of the multimode cladding material as well as its refractive index profile that is turned out through changes in waveguide properties of the fiber [27]. In terms of nonlinearity properties, especially for short length fibers, it may be also more useful to opt for holding the temperatures down at some value as better results have been achieved for shorter lengths.

The main reason why the thermal loading is so harmful is that it has its maximal value just at the pumped fiber end before it decreases fast. Figure 3 shows temperature distribution functions along the z axis, for r = b, for 3 different constant absorption coefficients. The absorption coefficients that have been used are: $\alpha_1 = 0.4$, $\alpha_2 = 0.1$, and $\alpha_3 = 0.01$, while the other parameters used during the calculations are represented in

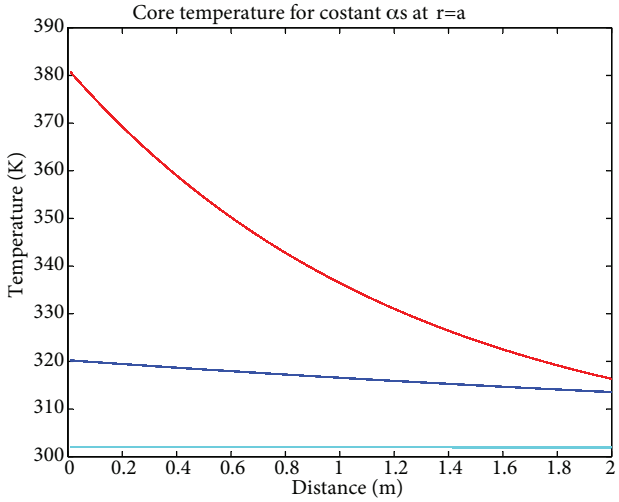


**Figure 3.** Temperature distribution functions in the forward-end pumped fiber laser at r = b for three absorption coefficients with constant values. The pumping and the lasers beams propagate in z direction of cylindrical coordinate.

the Table. It is to be noted that the fibers used for calculation of temperature profiles are the fibers available in the market.

**Table.** Parameters used in calculations.

| Parameter | Amount | Unit |
|---|---|---|
| a | 12.5 | $\mu$m |
| b | 125 | $\mu$m |
| $k_c$ | 23 | W/mK |
| $P_{in}$ | 100 | W |
| $T_c$ | 300 | K |
| $h_c$ | 50 | $W/m^2K$ |
| $k_f$ | 230 | W/mK |
| L | 2 | m |
| n | 400 | |
| $\lambda_p$ | 976 | nm |
| $\lambda_p$ | 1060 | nm |

According to Figure 3, it is quite certain that an increase in absorption coefficient causes higher maximum temperature reached at the pumping side of the fiber laser. At the same time, a higher absorption coefficient provides a more significant drop in temperature along the fiber. On this basis, it can be deduced that some increasing absorption function may not only cause a reduction in the temperature but also give the possibility of keeping the $T_1(r,z)$ or $T_2(r,z)$ under some temperature value along the fiber.

In order to support this opinion as well as achieve minimal thermal rise along the z axis the absorption coefficients, which rise between 0.01 and 0.4, are represented by modified logarithm, modified exponential and linear functions, respectively. The functions are given in polynomial forms given below and also represented in Figure 4.a [47].

$$\begin{aligned}
\alpha_1(z) &= -0.0081z^5 + 0.0814z^4 - 0.1628z^3 + 0.1747z^2 - 0.0237z + 0.01 \\
\alpha_2(z) &= 0.0326z^5 - 0.179z^4 + 0.4036z^3 - 0.5651z^2 + 0.6221z + 0.01 \\
\alpha_3(z) &= 0.195z + 0.01
\end{aligned}$$

Figure 4.b shows temperature distribution functions for 3 different variable coefficients, represented in Figure 4.a. Generally, all of the results show important temperature drop, verifying the idea that doping management can be used in thermal management. At the same time, as the final temperature is smaller than the long-term operation one, it can be also concluded that the final value of the absorption coefficient may be larger than the opted one. The results represented in Figure 4.b show that the best temperature drop is provided for the third polynomial.

According to power scaling behavior, the power drop for constant absorption coefficient, whose numerical calculations are represented in Figure 5.a, it can be deduced that a smaller absorption coefficient provides a smaller power drop also. However, increasing of doping level is important to minimize the gain length that consequently minimizes nonlinear effects. On the other hand, comparing just variable coefficients, whose results are represented in Figure 5.b, it can be said that the smallest power drop has been recorded for the third polynomial. Although all power drops recorded at the end of the fiber are small, the approach needs careful optimization.

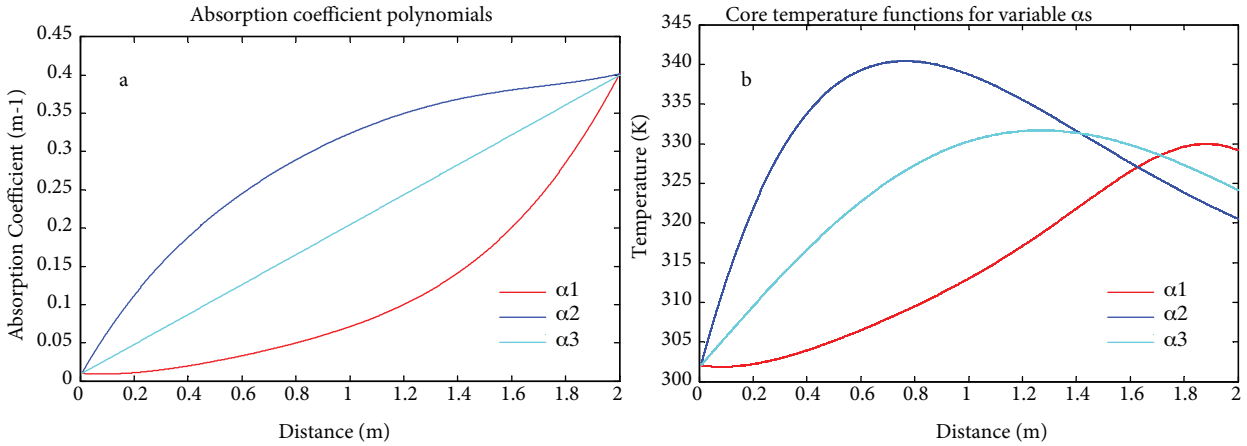


**Figure 4.** (a) Different increasing absorption coefficient functions used in calculations (b) Temperature distribution functions in the forward-end pumped fiber laser at r = b for three absorption coefficients with variable values, given as polynomials. The pumping and the lasers beams propagate in z direction of cylindrical coordinate.

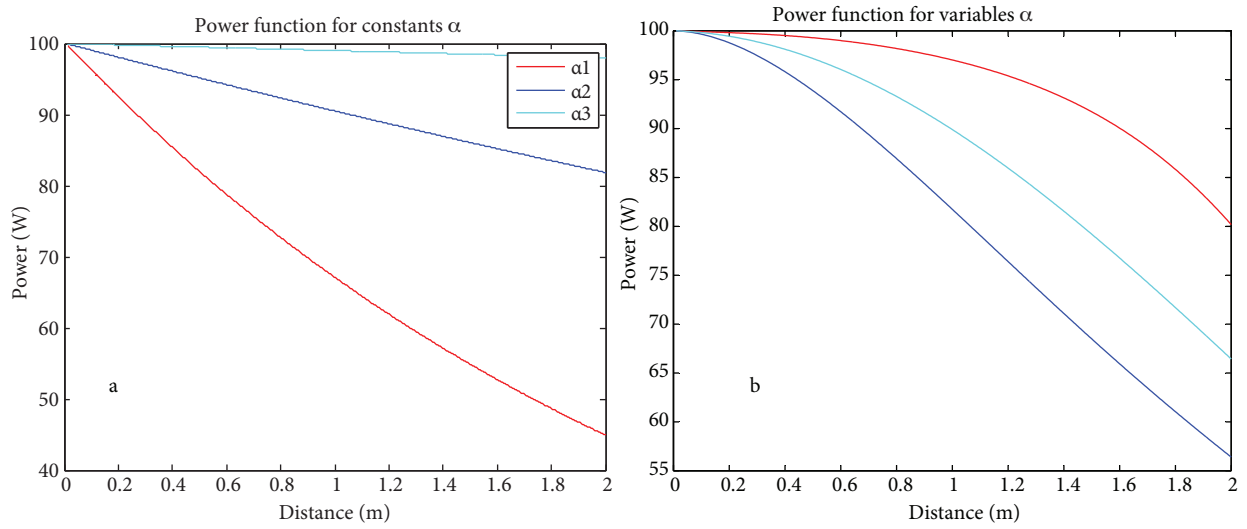


**Figure 5.** (a) Power distribution functions in the forward-end pumped fiber laser along $z$ axis for 3 different absorption coefficients with constant values. (b) Power distribution functions in the forward-end pumped fiber laser along $z$ axis for 3 different variable absorption coefficients presented as 3 different polynomials.

## 5. Conclusion

In this work, we proposed doping management, where the doping level of the gain fiber is varied continuously in the axial direction to minimize thermal load as well as mitigate the trade-off between thermal load and nonlinear processes concurrently keeping power scaling under control. In this work, at first we have constructed a heat dissipation model for double-clad fiber lasers with a top-hat pump beam with cooling at the outer cladding surface and analytically solved 3-D heat transfer functions for variable absorption coefficient. According to the analysis, we have presented graphs for both different constant and variable absorption coefficients as well as absorption coefficient function for constant temperature along the z axis.

The calculations show that gradually rise of the absorption coefficient causes a remarkable reduction in temperatures at the core and clad of the fiber laser. In terms of thermal considerations, it can be said that the

best results have been achieved for the third polynomial as the maximal achieved temperature is approximately 330 K, which is a significant reduction in regards to the anticipated value.

The numerical results also show that the third dimension in the thermal analysis of any type of high-power fiber lasers cannot be ignored. Moreover, it can be introduced as an active part of thermal control and may be a lifesaver of devastating temperatures at fiber cores.

Although our approach can readily be extended and improved upon with still nonexistent fibers, we think that it is theoretical verification of the experimental results presented by Elahi and colleagues obtained for different core and cladding diameter combinations of a 2 segment gain fiber.

## References

[1] Digonnet MJ. Rare-earth-doped fiber lasers and amplifiers revised and expanded. 2nd ed. New York, NY, USA: CRC Press, 2002.

[2] Müller HR, Kirchhof J, Reichel V, Unger S. Fibers for high-power lasers and amplifiers. CR Acad Sci II B 2006; 7/2: 154-162.

[3] Shiner B. The fibre laser: Delivering power. Nat Photonics 2010; 4/5: 290-290.

[4] Jauregui C, Limpert J, Tünnermann A. High-power fibre lasers. Nat Photonics 2013; 7/11: 861-867.

[5] Jeong YC, Boyland AJ, Sahu JK, Chung SH, Nilsson J, Payne DN. Multi-kilowatt single-mode ytterbium-doped large-core fiber laser. Journal of the Optical Society of Korea 2009; 13/4: 416-422.

[6] Smith AV, Do BT, Hadley GR, Farrow RL. Optical damage limits to pulse energy from fibers. IEEE J Sel Top Quant Elect 2009; 15/1: 153-158.

[7] Nilsson J, Jeong J, Codemard Y, Farrell CA, Vasquez C, Ji L, Abidin MSZ, van der Westhuizen G, Sahu JK. High power fibre lasers: Exploitation of unique properties. In: The European Conference on Lasers and Electro-Optics; 14-19 June 2009; Munich, Germany. OSA; pp. TF2_ 2.

[8] Varkey AV. Fiber based infrared lasers and their applications in medicine, spectroscopy and metrology. PhD, University of Michigan, Ann Arbor, Michigan, USA, 2013.

[9] Tunnermann A, Limpert J, Nolte S. Industrial perspectives of ultrafast fiber lasers. In: CLEOE-IQEC 2007 International Quantum Electronics Conference of Lasers and Electro-Optics; 17-22 June 2007; Munich, Germany. NY, USA: IEEE. pp.1-1.

[10] Nilsson J. High Power Fiber Lasers. In: CLEO/ QELS Quantum Electronics and Laser Science Conference; 16-21 May 2010; San Jose, CA. NY, USA: IEEE. pp. CTuC1.

[11] Richardson DJ, Nilsson J, Clarkson WA. High power fiber lasers: current status and future perspectives [Invited]. JOSA B 2010; 27/11: B63-B92.

[12] Nilsson J, Clarkson WA, Selvas R, Sahu JK, Turner PW, Alam SU, Grudinin AB. High-power wavelength-tunable cladding-pumped rare-earth-doped silica fiber lasers. Opt Fiber Technol 2004; 10/1: 5-30.

[13] Jeong Y, Vazquez-Zuniga LA, Lee SJ, Choi G, Kwon Y, Kim Y. High-Power Fiber Lasers. IEEE 17th Opto-Electronics and Communications Conference. 2-6 Jule 2012; Busan, South Korea. NY, USA: IEEE. pp. 580-581.

[14] Jeong Y, Nilsson J. Sahu JK, Dupriez P, Codemard CA, Soh DBS, Farrell C, Kim J, Richardson DJ, Payne DN. High Power Fiber Lasers. In: CLEO/Pacific Rim 2005 Optical Fiber Communication Conference; 30-02 August 2005; NY, USA: IEEE. pp. 1056-1058.

[15] Clarkson WA. Thermal effects and their mitigation in end-pumped solid-state lasers. J Phys D Appl Phys 2001; 34/16: 2381-2395.

[16] Li L, Li H, Qiu T, Temyanko VL, Morrell MM, Schülzgen A, Mafi A, Moloney JV, Peyghambarian N. 3-Dimensional thermal analysis and active cooling of short-length high-power fiber lasers. OSA. Opt Express 2005; 13/9: 3420-3428.

[17] Sahu JK, Jeong Y, Richardson DJ, Nilsson J. A 103 W erbium–ytterbium co-doped large-core fiber laser. P Soc Photo-Opt Ins 2003; 227:159-163.

[18] Bowman SR. Lasers without internal heat generation. IEEE J Quantum Elect 1999; 35/ 1: 115-122.

[19] Ueda K. High Power Fiber Lasers. In: CLEO/ Pacific Rim 4th Conference of Lasers and Electro-Optics; 15-19 July 2001; Chiba, Japan. NY, USA: IEEE. pp. 486-487.

[20] Wang Y, Xu CQ, Po H. Pump arrangement for kilowatt fiber lasers. In: LEOS 2003 16th Annual Meeting of the IEEE Lasers and Electro-Optics Society, 27-28 October 2003; NY, USA: IEEE. pp. 71-72.

[21] Liu X, Wang Y, Wang J, Zhang E, Xiong L, Zhao W. Development of diode lasers for pumping high power ultrashort pulse lasers. In: IEEE CLEO/PACIFIC RIM'09 Lasers and Electro-Optics Conference. 30-3 August 2009; Shanghai, China. NY, USA: IEEE. pp. 1-1.

[22] Zhu J, Zhou P, Ma Y, Xu X, Liu Z. Power scaling analysis of tandem-pumped Yb-doped fiber lasers and amplifiers. Opt Express 2011. 19/19: 18645-18654.

[23] Bowman SR, O'Connor SP, Biswal S, Condon NJ, Rosenberg A. Minimizing heat generation in solid-state lasers. IEEE J Quantum Elect 2010; 46/7: 1076-1085.

[24] Ashoori V, Shayganmanesh M, Radmard S. Heat generation and removal in solid state lasers. In: Salim NK. An Overview of Heat Transfer Phenomena, InTech, 2012. pp. 341-375.

[25] Konieczny P, Świderski J, Zając A, Skorczakowski M. Analysis of activation of active double-clad optical fibers. Opt Appl 2005; 35/ 4, 955-968.

[26] Fan Y, He B, Zheng JZ, Dai S, Zhao C, Wei Y, Lou Q. Efficient heat transfer in high-power fiber lasers. Chin Opt Lett 2012; 10/11: 111401-111401.

[27] Gainov VV, Shaidullin RI, Ryabushkin OA. Steady-state heating of active fibres under optical pumping. Quant Elect 2011; 41/7: 637-643.

[28] Tunnermann A, Schreiber T, Röser F, Liem A, Höfer S, Zellmer H, Nolte S, Limpert J. The renaissance and bright future of fibre lasers. J Phys B-At Mol Opt 2005; 38/S: 681-693.

[29] Limpert J, Roser F, Klingebiel S, Schreiber T, Wirth C, Peschel T, Ebrehardt R, Tunnermann A. The rising power of fiber lasers and amplifiers. IEEE J Sel Top Quant Elect 2007; 13/3: 537-545.

[30] Brown DC, Hoffman HJ. Thermal, stress, and thermo-optic effects in high average power double-clad silica fiber lasers. IEEE J Quantum Elect 2001; 37/2: 207-217.

[31] Yanming H, Cheo PK. Thermomechanical properties of high-power and high-energy Yb-doped silica fiber lasers. IEEE Photonic Tech L 2004; 16/3: 759-761.

[32] Canat G, Jaouën Y. Evidence of thermal effects in high power $Er^{3+}$-$Yb^{3+}$ fiber lasers. Opt Lett 2005; 30/22: 3030-3032.

[33] Li J, Duan K, Wang Y. Theoretical analysis of the heat dissipation mechanism in $Yb^{+3}$-doped double-clad fiber lasers. J Mod Optic 2007; 55/3: 459-471.

[34] Li P, Zhu C, Zou S, Zhao H, Jiang D, Li G, Chen M. Theoretical and experimental investigation of thermal effects in a high power $Yb^{3+}$-doped double-clad fiber laser. OPT Laser Technol 2008; 40/2: 360-364.

[35] Liu T, Yang ZM, Xu SH. Analytical investigation on transient thermal effects in pulse end-pumped short-length fiber laser. Opt Express 2009; 17/15: 12875-12890.

[36] Ashoori V, Malakzadeh A. Explicit exact three-dimensional analytical temperature distribution in passively and actively cooled high-power fibre lasers. J Phys D Appl Phys 2011; 44/35: 1-6.

[37] Assad MEH, Brown DC. Thermodynamic analysis of end-pumped fiber lasers subjected to surface cooling. IEEE J Quantum Elect 2013; 49/1: 100-107.

[38] Elahi P, Yılmaz S, Akçaalan Ö, Kalaycıoğlu H, Öktem B, Şenel Ç, Ilday FÖ, Eken K. Doping management for high-power fiber lasers: 100 W, few-picosecond pulse generation from an all-fiber-integrated amplifier. Opt Lett 2012; 37/15: 3042-3044.

[39] Wang Y, Xu C, Po H. Thermal effects in kilowatt fiber lasers. IEEE Photonic Tech L 2004; 16/1: 63-65.

[40] Elahi P, Zare N. The analytical solution of rate equations in end-pumped fiber lasers with minimum approximation and temperature distribution during the laser operation. Acta Phys Pol A 2009; 116/4: 522-524.

[41] Liping Z, Liu H, Li X. Theoretical analysis of $Yb^{3+}$-doped double-clad fiber lasers using a new analytical method. Optik-International Journal for Light and Electron Optics 2013; 124/12: 1264-1268.

[42] Liao X, Huang C. Optimization of $Yb^{3+}$ -doped double-clad fiber lasers using a new approximate analytical solution. Opt Laser Technol 2011; 43/1: 55-61.

[43] Dong X, Lou Q, Zhou J. Comparison of Yb-doped fiber laser with one-end and double-end pumping configuration. Opt Laser Technol 2007; 39/4: 871-874.

[44] Desurvire E. Analysis of gain difference between forward-and backward-pumped erbium-doped fiber amplifiers in the saturation regime. IEEE Photonic Tech L 1992; 4/7: 711-714.

[45] Xue D. Three-dimensional simulation of the temperature field in high-power double-clad fiber lasers. Optik 2011; 122/10: 932-935.

[46] Goowin ET. Recurrence relations for cross-products of Bessel functions. Q J Mech Appl Math 1948; 2/1: 73-74.

[47] Gursel AT, Elahi P, İlday FÖ, ÖzyazıcıMS. Theoretical analysis of doping management. In: IEEE ELECO 2013 8th Electrical and Electronics Engineering International Conference. 28-30 November 2013; Bursa, Turkey. NY, USA: IEEE. pp. 609-613.